

Direct observation of ultra-slow uncorrelated polaron dynamics in $\text{LaMnO}_{3+\delta}$

A.M.L. Lopes,^{1,2,*} J.P. Araújo,³ J.J. Ramasco,³ E. Rita,^{1,4} V.S. Amaral,²
J.G. Correia,¹ R. Suryanarayanan,⁵ and the ISOLDE Collaboration¹

¹*CERN EP, CH 1211 Geneve 23, Switzerland.*

²*Departamento de Física and CICECO, Universidade de Aveiro, 3810-193 Aveiro, Portugal.*

³*Departamento de Física, IFIMUP and CFP, Universidade do Porto, 4169-007 Porto, Portugal.*

⁴*ITN, E.N. 10, 2686-953 Sacavém, Portugal.*

⁵*Laboratoire de Physico-Chimie et de l'Etat Solide, Université Paris-Sud, 91405 Orsay, France.*

(Dated: May 23, 2019)

This letter reports a real-lattice atomic scale study on the $\text{LaMnO}_{3.12}$ compound using $\gamma-\gamma$ PAC spectroscopy. A thorough analysis of the PAC spectra revealed a continuous phase transition with two distinct local symmetries coexisting in a broad range of temperatures. The order-parameter β exponent hints for the free percolative nature of this transition, with the percolation thresholds delimiting the narrow range of temperatures where the average lattice symmetry presents Rhombohedral/Orthorhombic phase coexistence. The dynamics of the distorted local phase was studied via EFG fluctuations evidencing an ultra-slow thermal activated motion with an activation energy $E_a \approx 0.31$ eV, close to the Jahn-Teller small polaron binding energy. The free percolative nature of the transition suggests the uncorrelated dynamics of lattice distortions compatible with the presence of a polaron gas.

PACS numbers: 75.47.Lx, 76.80.+y, 64.60.Ak, 31.30.Gs

Intense experimental and theoretical work has been devoted to manganite systems due to its colossal magnetoresistance (CMR) and the richness of their local phenomena owing to the strong interplay of charge, lattice, orbital and spin degrees of freedom. The macroscopic crystal structure of these systems derives from the cubic perovskite ABO_3 , where Mn occupies the B-sites and the A-sites are occupied by a rare-earth (La, Pr, Nd...). The un-doped LaMnO_3 (LMO) compound is an antiferromagnetic insulator ($T_N = 140$ K) with cooperative distortion of MnO_6 octahedra caused by the static Jahn-Teller (JT) effect of the Mn^{3+} ion. Oxygen excess (cationic vacancies) or the presence of divalent ions at A-sites (Ca, Sr, Ba) reduces the static JT distortion due to the creation of Mn^{4+} ions, so favoring the ferromagnetic interaction and dynamic electron transfer between Mn^{3+} and Mn^{4+} ions. This interaction is known as double-exchange (DE) [1]. Although explaining qualitatively the CMR effect, this framework is insufficient to explain the mechanism responsible for the large resistivity of the paramagnetic insulator (PI) phase and other peculiar transport properties. Additional phenomena like strong electron-lattice coupling, leading to charge localization via JT distortions favoring polaron formation, should play a crucial role in doped manganites [2]. Experimental evidence for the existence of polarons was given by [3, 4, 5] and it is becoming recognized the important role played by such lattice distortions in the physics of these systems. In spite of these extensive studies, the mechanism of polaron dynamics and its relation with average lattice symmetry is still a matter of intense research [6, 7, 8].

Low doped manganites present even further unusual and nontrivial features. These include local inhomogeneities with phase segregation in nanoclusters,

strong electron-lattice coupling and a peculiar ferromagnetic insulator (FI) state [9]. In addition, manganites often show structural phase transitions (e.g. Orthorhombic-Rhombohedral), around which commonly emerge phase coexistence at the nanoscopic scale (nanoclusters). Whether structural phase transitions can be related to polaron formation is still an open issue. Structure of clusters, polaron dynamics and how far does phase coexistence extend are other important unsolved questions at the nanoscale level. Further insight in these topics can be achieved by real-lattice atomic scale studies with direct measurements of the local distortions and their dynamics. This type of measurements is accessible only for a few techniques, among which nuclear hyperfine methods have proved to be powerful tools to sample local atomic environments [10, 11]. In particular, Perturbed Angular Correlation (PAC) provides a sensitive method to detect Electrical Field Gradient (EFG), Magnetic Hyperfine field (MHF) and their fluctuations occurring during time scales ranging from ns to μ s (PAC time scale). In this way, PAC allows a direct estimation of the correlation times of EFG and MHF fluctuations with the advantage that PAC efficiency is temperature independent, allowing accurate measurements in a wide range of temperatures.

In this work $\gamma-\gamma$ PAC spectroscopy was used to monitor $^{111\text{m}}\text{Cd}-^{111}\text{Cd}$ implanted probes into doped LMO, to study its local environment and associated lattice dynamics. Cd occupies La sites, which are ideal positions to probe lattice distortions in the surrounding MnO_6 octahedra. Polycrystalline samples were produced by solid state reaction method. In order to perform PAC measurements, samples were implanted at room temperature with $^{111\text{m}}\text{Cd}$ ($T_{1/2} = 48$ min) to a homogeneous low dose

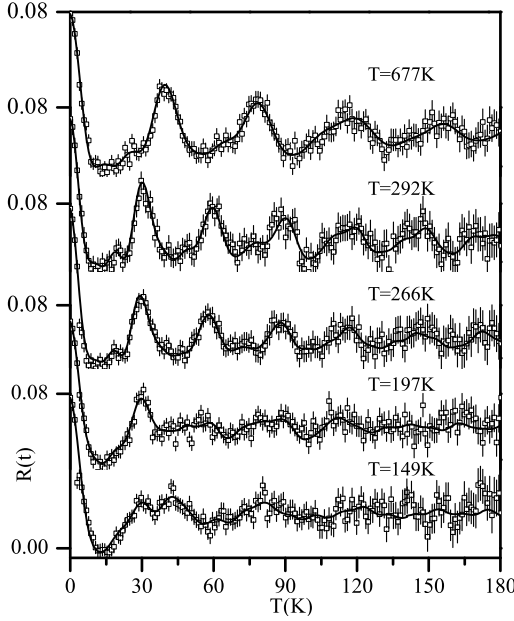


FIG. 1: Representative $\text{LaMnO}_{3.12}$ $R(t)$ experimental function and correspondent fits, as described in the text.

of 10^{12} cm^{-2} and 60 keV energy at the ISOLDE/CERN facility. After implantation the samples were annealed at 700°C in flowing O_2 during 20 minutes to allow recovery from implantation damage. The average lattice was monitored by powder x-ray diffraction measurements in a $80 - 500 \text{ K}$ temperature range. Transport and magnetization results showed an insulator ferromagnetic behavior with a Curie-Weiss temperature, $T_c \approx 145 \text{ K}$ and $\theta_p \approx 167 \text{ K}$ in close agreement with Refs [12, 13]. The PAC experimental perturbation functions, $R(t)$, were measured from 10 to 800 K using a high efficiency 6-BaF₂-detector spectrometer [14].

The PAC probe state, intermediate state of the $^{111}\text{mCd} \rightarrow ^{111}\text{Cd}$ cascade ($T_{1/2} = 84 \text{ ns}$, $I = 5/2$), is coupled to the EFG tensor V_{ij} through its quadrupole moment Q . The static nuclear Hamiltonian for the electric quadrupolar interaction, in the proper reference frame of V_{ij} with $|V_{zz}| \geq |V_{yy}| \geq |V_{xx}|$, is given by [15]

$$\mathcal{H}_Q = \hbar \omega_Q \left[3 I_z^2 - I(I+1) + \frac{1}{2} \eta (I_+^2 + I_-^2) \right] \quad (1)$$

Where $\omega_Q = eQV_{zz}/(4I(2I-1)\hbar)$ is the quadrupolar frequency, I stands for the probe nuclear spin and $\eta = (V_{xx} - V_{yy})/V_{zz}$ is the EFG asymmetry parameter. For spin $I = 5/2$, three transition frequencies ω_n , eigenvalues of \mathcal{H}_Q , are observable per EFG tensor. The PAC $R(t)$ function for such quadrupolar static hyperfine interaction

can be expressed as [15]

$$R(t) = A_{kk} G_{kk}(t) = A_{kk} \sum_{n=0}^3 S_{k_n} \cos(\omega_n t) e^{-\delta \omega_n t}, \quad (2)$$

where A_{kk} are the angular correlation coefficients and the perturbation factor $G_{kk}(t)$ depends only on the interactions the probe atoms are subjected to. The exponential term in Eq. (2) reflects the existence of static distribution of frequencies, here assumed as Lorentzian with average value ω_Q and FWHM, $\sigma_Q = 2\omega_Q\delta$, which accounts for the attenuation of the $R(t)$ function (line broadening). Another mechanism responsible for $R(t)$ attenuation is the existence of time-dependent interactions. If EFG fluctuations occur with a time scale comparable with the life time of the intermediate state, time dependent hyperfine interactions must be considered, as described by Blume stochastic theory [16]. However when dynamic effects produce fluctuations of orientation, strength and symmetry of EFG, the application of Blume's theory is cumbersome. Baubry [17] showed that if several jumps take place during the precession time, $\sim 2\pi/\omega_Q$, the $R(t)$ function may be satisfactorily described by a single exponential damping term, $e^{-\lambda t}$ multiplying the static expression (2), where $\tau_r \propto \lambda/\omega_Q^2$ is the average residence time in each state.

In Figure 1 representative $R(t)$ experimental functions for several temperatures are shown. As can be seen the spectra strongly change with lowering temperature. Data analysis has revealed that the PAC probes interact with two main EFG distributions which coexist over all temperature range. Above RT an almost axially symmetric local environment EFG_A ($V_{zz}^A \approx 111 \text{ V/\AA}^2$ and $\eta_A \approx 0.15$, typical values around RT) predominates while at low temperatures mainly a weaker highly asymmetric EFG_B ($V_{zz}^B \approx 60 \text{ V/\AA}^2$ and $\eta_B \approx 0.78$) exists. A temperature independent small contribution, $\sim 5\%$, of a third EFG_C distribution was also found and it is probably related to probes located at grain boundaries. Note that, above T_c , no MHF contributions are present allowing a very accurate quantification of the different local EFG components (A, B, C) and their corresponding global fractions. Figure 2 shows the fraction of probes interacting with each EFG component (f_A, f_B, f_C) as a function of temperature. A remarkable feature of this result is the persistence, up to very high temperatures, of the B component compatible with the scenario of random distributed nanoscopic regions of a highly distorted lattice (EFG_B) embedded in a more symmetric matrix (EFG_A). Lowering T , the fraction of probes interacting with the A component continuously decreases till a remanent value $r_A \sim 10\%$ at low temperatures. This smooth variation of f_A (and symmetrically f_B) suggests the presence of a continuous phase transition between a local environment dominated by A component and other with a dominant B component. The order parameter of a continuous tran-

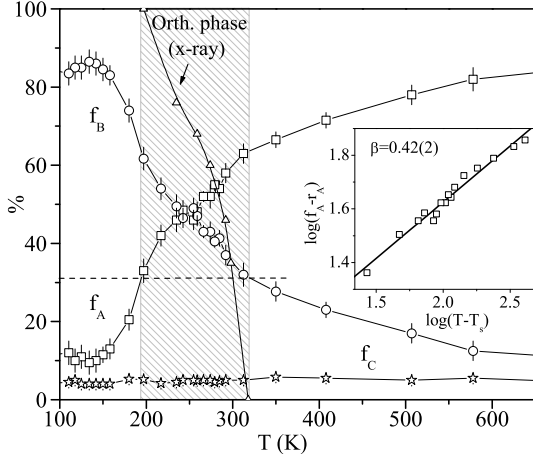


FIG. 2: Temperature dependence of the fraction probes interacting with the different EFG. Triangles represent the fraction of orthorhombic phase obtained using x-ray diffraction technique. The dashed line is a guidelines assigning the percolation threshold. The inset shows a log-log plot of $(f_A - r_A)$ against the deviation to the critical temperature T_s to estimate the order-parameter β exponent.

sition follows $f_A - r_A \sim (T - T_s)^\beta$, where β is a critical exponent and T_s is the transition temperature. As shown in the inset of figure 2 a critical $T_s = (170 \pm 10) K$ and $\beta = 0.42 \pm 0.02$ were found. The estimated β is remarkably close to the exponent of free percolation on a 3D cubic lattice ($\beta_p = 0.41$ [18]). Such continuous phase transition exhibits a diverging correlation length when the critical point is approached, $\xi \sim |T - T_s|^{-\nu}$. In the present case, this correlation length may be associated to the mean size of the nanoscopic aggregates (i.e. local B type distortions or nanoclusters inside a dominant A phase). Since the measured exponent β is related to free percolation, clusters must percolate at $f_B = 31.16\%$ [18], symmetrically at the same value of f_A when T is rising. Indeed, and in agreement with refs. [12, 19], our x-ray measurements detect a structural phase transition (orth-rhomb) with phase coexistence ranging precisely between these two percolation thresholds as assigned in Fig. 2 (shaded zone). The fact of x-rays measurements not finding a phase coexistence outside this zone though PAC detects a relatively high percentage ($\sim 10 - 30\%$) of the invading component may be explained by the fractal and/or dynamic nature of clusters.

Dynamic effects manifest in the time-dependent attenuation parameter, λ_B , of the non-symmetric EFG $_B$. In fact, below 400 K the attenuation of EFG $_B$ to the $R(t)$ fit function shows a pronounced increase peaking at 266 K. This effect can be directly attributed to EFG fluctuations occurring in a time scale within the PAC time window ($1 - 800 ns$). A complete sketch of dynamic and static attenuation to $R(t)$ is depicted in figure 3. As can be seen, since EFG fluctuation rates are extremely fast at

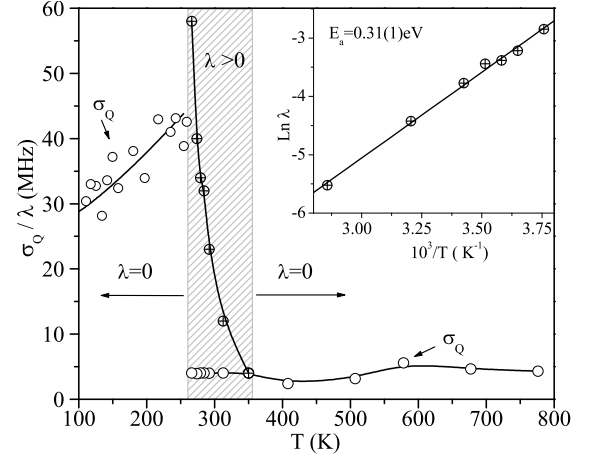


FIG. 3: Static (o) and dynamic (\oplus) attenuation parameters to the $R(t)$ experimental function for the f_B component against temperature. The dynamic attenuation parameter is plotted in the inset in a log-normal scale (Arrhenius plot) to estimate the activation energy.

high temperatures, PAC measure only an ensemble average frequency ω_Q^B with a attenuation parameter produced by the static disorder (σ_Q^B). Lowering T , the dynamics of the local distortions retards, becoming thus measurable within our experimental time window. Thus λ_B increases till the polaron jump frequency-rate becomes of the same order of the quadrupole interaction (EFG $_B$) observable frequency, $\omega_{pol} \approx \omega_Q^B$. This tendency breaks down for lower temperatures when polaron dynamics becomes slower than ω_Q^B . In this limit, the attenuation to the $R(t)$ function is again fully accounted by σ_Q^B .

We further point that the dynamics associated with the B component participates of the thermal activated motion proper of small polarons ($\lambda_B = \lambda_\infty e^{E_a/kT}$), as can be seen in the inset of figure 3. As stated above, $\lambda_B = const. \tau_r \langle \omega_Q^B \rangle^2$ and since ω_Q^B is almost constant in the region of interest (Fig. 4), the activation energy (E_a) of the lattice dynamic process can be deduced from the temperature dependence of the attenuation parameter λ_B . The value of E_a determined in this way for the B component was found to be $0.31 eV$, similar to the small polaron binding energy reported in the literature for low doped manganites [8, 20, 21]. This value contrasts with that found in [10], probably due to the intense magnetic field (7 T) needed to perform NMR measurements. On the other hand, τ_r can be obtained if the proportionality constant between λ_B and τ_r is determined. In the Abragam-Pound limit [22] for spin 5/2 we have that $const. = 16/n$, where n is the number of possible EFG states. If one considers that a polaron can be formed in any of the 8 octahedra around a La site ($n \approx 8$), $\tau_r = 0.5 \mu s$ at $T = 266 K$. Note that this value of τ_r corresponds to an ultra-slow polaron dynamics, compatible

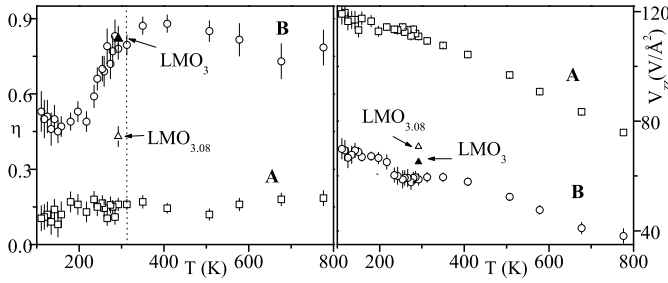


FIG. 4: EFG principal component, V_{zz} , (right) and asymmetry parameter, η , (left) for the A and B phases of $\text{LaMnO}_{3.12}$ as a function of the temperature. EFG parameters measured at RT for $\text{LaMnO}_{3.08}$ and LaMnO_3 are also showed.

with the insulator behavior of this sample.

Contrarily to what happens with the B component, EFG fluctuations are not detected for the more symmetric EFG_A , where no significant changes in the static attenuation parameter are observed. This behaviour suggests that polaron might not form on the more symmetric A phase. As can be seen in figure 4 the symmetry of A phase is higher and does not vary appreciably with temperature ($\eta_A \approx 0.15$). Furthermore the principal component of EFG V_{zz}^A slight decreases with increasing of temperature, a typical feature of perovskite and similar systems. This behavior is normally attributed to thermal lattice expansion and lattice vibrations. Although V_{zz}^B has a similar tendency as V_{zz}^A , the asymmetry parameter η_B shows a significant decrease below 312K that precisely corresponds to the percolation threshold quoted above. The high η_B value at high T points to a strong distorted local environment for isolated nanoclusters. Such EFG parameters compare extremely well with the cooperative JT distorted LaMnO_3 measured at RT, triangles in the Fig 4, further suggesting that the observed B distortions are JT polarons. At temperatures below the percolation threshold the η value decreases pointing to a lower distorted environment for the B component when the orth. crystallographic phase dominates, i.e. when $f_B \geq 50\%$. In this regime, the EFG parameters agree with those also measured at RT for the weakly JT distorted $\text{LaMnO}_{3.08}$, triangles in Fig. 4.

It was further seen that below T_C both A and B local environments experience increasing MHFs upon decreasing temperature, presenting at 10K values of $B_A = 4.0(3)T$ and $B_B = 3.8(2)T$, compatible with a fully ferromagnetic environment [10, 24]. In this way, a ferromagnetic phase (f_B) with slow uncorrelated Jahn-Teller polarons (insulator) competes with a remanent non-distorted ferromagnetic phase (f_A), probably metallic, as observed in similar systems [23].

In conclusion $\gamma - \gamma$ PAC technique has been applied to study $\text{LaMnO}_{3.12}$ local environment and associated lattice dynamics. A continuous structural phase transition

between a local symmetric environment, phase A, and a highly asymmetric, phase B was found. The value of the estimated β exponent hints to the free percolation nature of the transition. The two local phases coexist within a broad range of temperatures, though their detection by x-rays measurements is only possible within a narrow T window constrained between the A and B percolation thresholds. The dynamic aspect of the transition was also examined hinting that at high T , the B distortions, polarons, diffuse inside the dominant A phase. Lowering temperature, polaron dynamics slows down and the fraction of B phase increases. The observed free percolative character of the transition implies that the interactions between polarons must be negligible, pointing to the presence of a polaron gas. Additionally, below T_C the two phases become ferromagnetic, suggesting phase coexistence between a FMI and FMM regions.

The authors are grateful to W. Troeger, F. Heinrich and J.M. Vieira for useful discussions and technical support. This work was funded by the Portuguese Research Council (FCT), ESF (projects POCTI/CTM/35462/00, POCTI/FNU/49509/2002) and EU (Large Scale Facility contract HPRI-CT-1999-00018). A.M.L. Lopes, J.J. Ramasco and E. Rita acknowledge their grants to FCT.

* Electronic address: armandina.lima.lopes@cern.ch

- [1] C. Zener *et al.* Phys. Rev. **82**, 403 (1951).
- [2] A.J. Millis, P.B. Littlewood and Boris I. Shraiman, Phys. Rev. Lett. **74**, 5144 (1995).
- [3] S.J.L. Billinge *et al.* Phys. Rev. Lett. **77**, 715 (1996).
- [4] G. Zhao *et al.* Nature **381**, 676 (1996).
- [5] Despina Louca *et al.* Phys. Rev. B **56**, R8475 (1997).
- [6] V. Kiryukhin *et al.* Phys. Rev. B **67**, 064421 (2003).
- [7] L. Martín-Carrón *et al.* Phys. Rev. B **66**, 174303 (2002).
- [8] N. Mannella *et al.* Phys. Rev. Lett. **92**, 166401 (2004).
- [9] E. Dagotto *et al.* Phys. Reports **344**, 1-153 (2001).
- [10] G. Allodi *et al.* Phys. Rev. Lett. **87**, 127206 (2001).
- [11] R.H. Heffner *et al.* Phys. Rev. Lett. **85**, 3285 (2000).
- [12] C. Ritter *et al.* Phys. Rev. B **56**, 8902 (1997).
- [13] F. Prado *et al.*, J. Sol. Sta. Chem. **146**, 418 (1999).
- [14] T. Butz *et al.*, Nucl. Instr. Meth. A **284**, 417 (1989)
- [15] G. Schatz and A. Weidinger, *Nuclear Condensed Matter Physics*, John Wiley & Sons England (1996).
- [16] M. Blume, Phys. Rev. **174**, 351 (1968)
- [17] A. Baubry and P. Boyer, Hyp. Int. **25**, 803 (1987)
- [18] D. Stauffer and A. Aharony, *Introduction to percolation theory*, Taylor & Francis (1991).
- [19] F. Prado *et al.*, J. Matter. Chem. **10**, 2139 (1997)
- [20] A. Weisse, J. Loos and H. Fehske, Phys. Rev. B **68**, 024402 (2003)
- [21] J.S. Zhou, J.B. Goodenough, Phys. Rev. B **68**, 144406 (2003)
- [22] H. Winkler and E. Gerdau, Z. Physik. **262**, 363 (1973)
- [23] M.M. Savosta *et al.*, Phys. Rev. Lett. **87**, 137204 (2001), and J. Exp. Theor. Phys. **97** 573 (2003)
- [24] M. K. Gubkin *et al.*, J. Mag. Mag. Mat. **154**, 351 (1996)